


## Ruthenium(II) bipyridine complexes: From synthesis and crystal structures to electrochemical and cytotoxicity investigation

Afya A. Baroud, Ljiljana E. Mihajlović-Lalić, Nevenka Gligorijević, Sandra Aranđelović, Dalibor Stanković, Siniša Radulović, Kristof Van Hecke, Aleksandar Savić & Sanja Grgurić-Šipka

To cite this article: Afya A. Baroud, Ljiljana E. Mihajlović-Lalić, Nevenka Gligorijević, Sandra Aranđelović, Dalibor Stanković, Siniša Radulović, Kristof Van Hecke, Aleksandar Savić & Sanja Grgurić-Šipka (2017): Ruthenium(II) bipyridine complexes: From synthesis and crystal structures to electrochemical and cytotoxicity investigation, Journal of Coordination Chemistry, DOI: [10.1080/00958972.2017.1282611](https://doi.org/10.1080/00958972.2017.1282611)

To link to this article: <http://dx.doi.org/10.1080/00958972.2017.1282611>

 [View supplementary material](#) 

 Accepted author version posted online: 17 Jan 2017.

 [Submit your article to this journal](#) 

 Article views: 3

 [View related articles](#) 

 [View Crossmark data](#) 

**Publisher:** Taylor & Francis

**Journal:** *Journal of Coordination Chemistry*

**DOI:** <http://dx.doi.org/10.1080/00958972.2017.1282611>

## **Ruthenium(II) bipyridine complexes: From synthesis and crystal structures to electrochemical and cytotoxicity investigation**

AFYA A. BAROUD†, LJILJANA E. MIHAJLOVIĆ-LALIĆ‡, NEVENKA GLIGORIJEVIĆ§, SANDRA ARANĐELOVIĆ§, DALIBOR STANKOVIĆ‡, SINIŠA RADULOVIĆ§, KRISTOF VAN HECKE¶, ALEKSANDAR SAVIĆ\*† and SANJA GRGURIĆ-ŠIPKA\*†

†Faculty of Chemistry, University of Belgrade, Studentski trg 12-16, 11 000 Belgrade, Serbia

‡Innovation Center of the Faculty of Chemistry, University of Belgrade, Studentski trg 12-16, 11 000 Belgrade, Serbia

§Institute for Oncology and Radiology of Serbia, Pasterova 14, 11000 Belgrade, Serbia

¶XStruct, Department of Inorganic and Physical Chemistry, Ghent University, Krijgslaan 281-S3, B-9000 Ghent, Belgium

Complexes **1-4**,  $[\text{Ru}(\text{L})(\text{bpy})_2]\text{PF}_6$ , where bpy = 2,2'-bipyridine; L = 3-methylpyridine-2-carboxylic acid (**L1**), 6-methylpyridine-2-carboxylic acid (**L2**), 5-bromopyridine-2-carboxylic acid (**L3**) and 6-bromopyridine-2-carboxylic acid (**L4**), were synthesized and characterized. The electrochemical character of the complexes was investigated by cyclic voltammetry revealing two reversible reduction waves in the negative range of potentials, most likely due to a reduction of the bipyridine moiety. Cytotoxicity studies by MTT assay for 72 h of drug action revealed that **2-4** exhibited moderate activity in cervical human tumor cells (HeLa). Complex **2** exhibited low activity in colon cancer LS-174 cells ( $180 \pm 10$ ), while all complexes were devoid of activity in lung cancer A549 and non-tumor MRC-5 cells, up to 200  $\mu\text{M}$ . Combinational studies of the most active complex **2**, with pharmacological modulators of cell redox status, L-buthionine-sulfoximine (L-BSO) or N-acetyl-L-cysteine (NAC), showed that when L-BSO potentiated, **2** induced a sub-G1 peak of the cell cycle in the HeLa cell line. UV-vis and cyclic voltammetry were performed in order to investigate the binding mode of **2** to DNA and suggested intercalation for the complex-DNA interaction.

---

\*Corresponding authors. Email: sanjag@chem.bg.ac.rs (S. Grgurić-Šipka); aleksandar@chem.bg.ac.rs (A. Savić)

*Keywords:* Ruthenium(II) bipyridine complexes, Crystal structure, Redox properties, Cytotoxicity, DNA Intercalation

## 1. Introduction

Metal-based drugs have potential in inorganic medicinal chemistry [1-3]. The greatest revolution was made by Rosenberg's discovery of *cisplatin*'s cytotoxicity [4, 5]. A large number of scientists have been inspired to design compounds that would eventually resolve well-known limitations of commercial drugs (resistance and side effects) [6]. A few thousand compounds bearing diverse metals and ligand systems have been synthesized [7-11]. Considering that only *carboplatin* and *oxaliplatin* broaden the platinum-based drugs series [12, 13], alternative approaches are needed. The use of group-8 metal (ruthenium and osmium) complexes leads to significant progress [14, 15]. Ruthenium and osmium offer different oxidation states (+2 and +3) and redox chemistry. Additionally, their ligand exchange properties and suitable binding to biomolecules positively affect the overall mode of action [16]. So far, two Ru complexes (NAMI-A and KP1019) have undergone clinical trials [17, 18]. As modern cancer therapy imposes even more rigid criteria for the final clinical use, the whole metal drug concept is subject to significant change. Thus, every extensive study includes the synthetic route followed by structural and electrochemical characterization, *in vitro* and DNA targeting tests as well as examination of protein inhibition.

Selecting a suitable metal-ligand framework certainly represents the promising base of the research. Literature data suggest rather few metals (ruthenium, osmium and gold) that are still attractive [11, 19, 20]. The metal center and its oxidation state dictate the geometry of the complex, which directly impacts the kinetic inertness of a potential drug. Complexes having metals in higher oxidation states act as prodrugs as they are reduced in blood and can be orally administered [21]. Then, the choice of the ligand system must be made. The ligand can be responsible for redox activity [22] as well as for anticancer activity [23, 24]. It can also improve the solubility of the complex, reduce toxicity and enhance specificity [25]. Some studies showed how low antitumor activity of the ligand can be improved by coordination to the metal center(s) [26, 27]. Others pointed out significant antitumor activity of pure organic species that later on were coordinated to metals [28]. From a strictly chemical point of view, metal-ligand synergism is important in designing the perfect drug structure.

The ligand carrier may originate from a structure that has a rather specific role in some biological systems. In that sense, some authors emphasize the significance of picolinic acid (2-pyridinecarboxylic acid) [29-31]. This six-membered ring molecule is found in mother's milk and has direct impact on mineral uptake in humans [32]. Besides its wide variety of physiological properties, picolinic acid is also an industrially significant compound, used as an active substance in a number of dietary supplements [33, 34]. Picolinic acid and its derivatives are present in the literature as multidentate ligands whose coordination modes rely on two different ligand atoms [35, 36]. Some Pt(II) [37] as well as Ru(II) complexes [38, 39] with this type of ligand were synthesized and proved to be active against various cell lines. Among Ru complexes, compounds bearing a 2,2'-bipyridine are also well recognized, not only as potential drugs but also as highly diverse photochemical and redox systems [22, 40]. Thus, combination of (electro)chemical properties makes them very attractive in terms of different potential applications (*e.g.* chemotherapy, catalysis) [41, 42].

Following expanding interest for this type of structure, a set of four ruthenium(II)-bipyridine complexes with methyl- and bromo-substituted derivatives of picolinic acid was prepared. The study also includes investigation of their electrochemical character and potential antitumor effect. Enhanced dependence of cancer cell on mitogenic and anti-apoptotic ROS-signaling represents a vulnerability that can be selectively targeted. Thus, agents that possess potential as direct/indirect-acting pro- or anti-oxidants may be candidates as redox chemotherapeutic agents. We investigated whether chemosensitization of HeLa tumor cells on the tested type of ruthenium agents may be obtained in combination with pharmacological modulators of cell redox-status, such as L-buthionine-S,R-sulfoximine (BSO), inhibitor of glutathione biosynthesis, or N-acetyl-cysteine (NAC), as a scavenger of reactive oxygen species (ROS).

## **2. Experimental**

### **2.1. Materials and physical measurements**

All experiments were performed under atmospheric conditions with commercially available chemicals and solvents used as received. In particular, **L1-L4** were purchased from Sigma Aldrich. The starting complex,  $[\text{RuCl}_2(\text{bpy})_2]$ , was synthesized according to a previously described but slightly modified synthetic route [43, 44].

Elemental analyses were performed on an Elemental Vario EL III microanalyzer. A Nicolet 6700 FT-IR spectrometer was used for recording infrared spectra. Signal intensities were reported with wavenumbers. LTQ Orbitrap XL Mass Spectrometer (Heated ESI) was used for recording all mass spectra in acetonitrile (HPLC grade) in a positive mode. The obtained peaks were assigned and interpreted according to dimensionless mass/charge ratio.  $^1\text{H}$  NMR spectra were recorded on a Bruker Avance III 500 spectrometer in DMSO with TMS as the reference. A rough estimation of the melting points was done using an electrothermal melting point apparatus.

Electrochemical measurements were performed with a CHI-760B instrument at room temperature. A three-electrode system consisted of a boron-doped diamond electrode (Windsor Scientific Ltd., Slough, Berkshire, United Kingdom) embedded in a polyether ether ketone (PEEK) body with an inner diameter of 3 mm, a resistivity of  $0.075\ \Omega\ \text{cm}$  and a boron doping level of 1000 ppm (as declared by the supplier), used as working electrode, a non-aqueous Ag/AgCl electrode used as the reference electrode and a platinum wire that was used as a counter electrode from  $-2.3\ \text{V}$  to  $1\ \text{V}$ . For the experiments,  $1.0\ \text{mM}$  solutions of the synthesized complexes in DMSO were prepared and TBAP was added as a supporting electrolyte. Cyclic voltammograms were obtained at  $20\ \text{mV}\ \text{s}^{-1}$  for **1-4** and  $50, 100, 150, 200, 300, 500\ \text{mV}\ \text{s}^{-1}$  for **4**.

## 2.2. Synthesis of the complexes

$[\text{RuCl}_2(\text{bipy})_2]$  (100 mg, 0.21 mmol) was dissolved in ethanol (15 mL) and stirred for 20 min at  $40\ ^\circ\text{C}$ . 3-Methylpyridine-2-carboxylic acid, **L1** (28.3 mg, 0.21 mmol) or 6-methylpyridine-2-carboxylic acid, **L2** (28.3 mg, 0.21 mmol) or 5-bromopyridine-2-carboxylic acid (41.7 mg, 0.21 mmol), **L3** or 6-bromopyridine-2-carboxylic acid **L4** (41.7 mg, 0.21 mmol) was dissolved in a small volume of ethanol (5 mL) and added to ethanol solution of the starting complex. The reaction mixture was stirred for 3 h under reflux and afterwards left to cool to room temperature. After adding an equimolar amount of a counterion,  $\text{NH}_4\text{PF}_6$  (33.7 mg, 0.21 mmol), dark red precipitate was isolated by filtration. The crude product was washed with a small amount of water and diethylether.

**2.2.1.  $[\text{Ru}(\text{L1})(\text{bpy})_2](\text{PF}_6)$  (**1**).** Yield: 71%.  $^1\text{H}$  NMR (500 MHz, DMSO- $d_6$ ),  $\delta$  (ppm): 8.81 (dd2H, Ar), 8.75-8.69 (m, 3H, Ar), 8.16 (q, 2H, Ar), 7.98 (p, 2H, Ar), 7.83-7.78 (m, 4H, Ar),

7.64 (t, 1H, Ar), 7.54 (br s, 1H, Ar), 7.39-7.33 (m, 4H, Ar), 2.67 (s, 3H, -CH<sub>3</sub>). IR (cm<sup>-1</sup>): 3423.2 (w), 1645.0 (s), 1446.8 (m), 1333.6 (m), 1268.0 (w), 1239.1 (w), 839.8 (vs), 766.2 (s), 730.7 (w), 558.2 (s). ESI-MS (*m/z*, (relative abundance, %)): 550.08 [M<sup>+</sup> - PF<sub>6</sub><sup>-</sup>, 100]. Anal. calcd for C<sub>27</sub>H<sub>22</sub>N<sub>5</sub>O<sub>2</sub>RuPF<sub>6</sub> · 0.5 H<sub>2</sub>O (%): C, 46.09; H, 3.30; N, 9.95. Found: C, 45.55; H, 3.44; N, 9.53. M.p.: above 300 °C.

**2.2.2. [Ru(L2)(bpy)<sub>2</sub>](PF<sub>6</sub>) (2).** Yield: 65%. <sup>1</sup>H NMR (500 MHz, DMSO-d<sub>6</sub>), δ (ppm): 8.82 (br t, 2H, Ar), 8.19 (br t, 2H, Ar), 8.08 (br s, 1H, Ar), 7.99 (sept, 2H, Ar), 7.94-7.85 (m, 4H, Ar), 7.82-7.78 (m, 2H, Ar), 7.62 (br t, 2H, Ar), 7.50-7.30 (m, 4H, Ar), 1.68 (s, 3H, -CH<sub>3</sub>). IR (cm<sup>-1</sup>): 3089.3 (w), 1650.4 (m), 1604.0 (m), 1466.8 (m), 1450.0 (m), 1159.3 (w), 840.5 (vs), 766.6 (s), 557.3 (s). ESI-MS (*m/z*, (relative abundance, %)): 550.08 [M<sup>+</sup> - PF<sub>6</sub><sup>-</sup>, 100]. Anal. calcd for C<sub>27</sub>H<sub>22</sub>N<sub>5</sub>O<sub>2</sub>RuPF<sub>6</sub> (%): C, 46.69; H, 3.19; N, 10.08. Found: C, 46.33; H, 3.28; N, 9.84. M.p.: above 300 °C.

**2.2.3. [Ru(L3)(bpy)<sub>2</sub>](PF<sub>6</sub>) (3).** Recrystallization of the amorphous product from an EtOH-ACN mixture gave deep red crystals suitable for X-ray analysis. Yield: 63%. <sup>1</sup>H NMR (500 MHz, DMSO-d<sub>6</sub>), δ (ppm): 8.82 (t, 2H, Ar), 8.74 (br q, 2H, Ar), 8.68 (d, 2H, Ar), 8.21 (p, 4H, Ar), 8.11 (d, 1H, Ar), 8.06-7.95 (m, 1H, Ar), 7.87 (dd, 1H, Ar), 7.80 (t, 1H, Ar), 7.64 (t, 1H, Ar), 7.55 (d, 1H, Ar), 7.51 (s, 1H, Ar), 7.38 (br t, 2H, Ar). IR (cm<sup>-1</sup>): 3080.5 (w), 1647.5 (s), 1603.4 (m), 1447.1 (m), 1373.7 (w), 1327.4 (w), 1160.5 (w), 1027.2 (w), 840.8 (vs), 767.9 (s), 727.5 (m), 556.0 (s), 506.1 (w). ESI-MS (*m/z*, (relative abundance, %)): 615.97 [M<sup>+</sup> - PF<sub>6</sub><sup>-</sup>, 100]. Anal. calcd for C<sub>26</sub>H<sub>19</sub>N<sub>5</sub>O<sub>2</sub>RuBrPF<sub>6</sub> (%): C, 41.12; H, 2.52; N, 9.22. Found: C, 40.75; H, 2.63; N, 9.38. M.p.: above 300 °C.

**2.2.4. Synthesis of [Ru(L4)(bpy)<sub>2</sub>](PF<sub>6</sub>) (4).** Recrystallization of the amorphous product from an EtOH-ACN mixture gave deep red crystals suitable for X-ray analysis. Yield: 38%. <sup>1</sup>H NMR (500 MHz, DMSO-d<sub>6</sub>), δ (ppm): 8.84 (t, 2H, Ar), 8.76-8.71 (m, 2H, Ar), 8.65 (dd, 2H, Ar), 8.39 (t, 1H, Ar), 8.33 (d, 1H, Ar), 8.26-8.20 (m, 1H, Ar), 8.09-7.78 (m, 4H, Ar), 7.68 (t, 1H, Ar), 7.43 (d, 1H, Ar), 7.38 (t, 1H, Ar), 7.34 (t, 1H, Ar), 7.27 (t, 1H, Ar), 7.17 (d, 1H, Ar). IR (cm<sup>-1</sup>): 3091.3 (w), 1647.4 (m), 1604.9 (w), 1449.8 (m), 840.9 (vs), 766.2 (s), 556.8 (m). ESI-MS (*m/z*,

(relative abundance, %): 615.97 [ $M^+ - PF_6^-$ , 100]. Anal. calcd for  $C_{26}H_{19}N_5O_2RuBrPF_6$  (%): C, 41.12; H, 2.52; N, 9.22. Found: C, 40.83; H, 2.75; N, 9.22. M.p.: above 300 °C.

### 2.3. Single-crystal X-ray diffraction

For the reported structures, X-ray intensity data were collected at 100 K on an Agilent Supernova Dual Source (Cu at zero) diffractometer equipped with an Atlas CCD detector using  $\omega$  scans and  $CuK\alpha$  ( $\lambda = 1.54184 \text{ \AA}$ ) radiation. The images were interpreted and integrated with CrysAlisPro (Rigaku Oxford Diffraction) [45]. Using Olex2 [46], the structures were solved by direct methods using the ShelXS structure solution program and refined by full-matrix least-squares on  $F^2$  using the ShelXL program package [47]. Non-hydrogen atoms were anisotropically refined and hydrogens in the riding mode and isotropic temperature factors fixed at 1.2 times  $U(eq)$  of the parent atoms (1.5 times  $U(eq)$  for methyl and hydroxyl groups).

*Crystal data for 3.*  $C_{30}H_{31}BrF_6N_5O_4PRu$ ,  $M = 851.54$ , monoclinic, space group  $P2_1/n$  (No. 14),  $a = 11.0258(2) \text{ \AA}$ ,  $b = 14.1182(3) \text{ \AA}$ ,  $c = 20.8563(5) \text{ \AA}$ ,  $\beta = 92.332(2)^\circ$ ,  $V = 3243.90(12) \text{ \AA}^3$ ,  $Z = 4$ ,  $T = 100 \text{ K}$ ,  $\rho_{calc} = 1.744 \text{ g cm}^{-3}$ ,  $\mu(Cu-K\alpha) = 6.531 \text{ mm}^{-1}$ ,  $F(000) = 1704$ , 31031 reflections measured, 6531 unique ( $R_{int} = 0.0731$ ) which were used in all calculations. The final  $R1$  was 0.0368 ( $I > 2\sigma(I)$ ) and  $wR2$  was 0.0993 (all data).

*Crystal data for 4.*  $C_{26}H_{19}BrF_6N_5O_2PRu$ ,  $M = 759.40$ , monoclinic, space group  $I2/a$  (No. 15),  $a = 18.0576(9) \text{ \AA}$ ,  $b = 18.0576(9) \text{ \AA}$ ,  $c = 21.4772(13) \text{ \AA}$ ,  $\beta = 109.681(6)^\circ$ ,  $V = 5213.9(5) \text{ \AA}^3$ ,  $Z = 8$ ,  $T = 100 \text{ K}$ ,  $\rho_{calc} = 1.935 \text{ g cm}^{-3}$ ,  $\mu(Cu-K\alpha) = 7.977 \text{ mm}^{-1}$ ,  $F(000) = 2992$ , 14143 reflections measured, 5079 unique ( $R_{int} = 0.0440$ ) which were used in all calculations. The final  $R1$  was 0.0462 ( $I > 2\sigma(I)$ ) and  $wR2$  was 0.1368 (all data).

### 2.4. Biology tests

**2.4.1. Reagents and cell cultures.** Human cervical adenocarcinoma (HeLa), human alveolar basal adenocarcinoma (A549), human colon cancer (LS-174), and human fetal lung fibroblast (MRC-5) cell lines were maintained as a monolayer culture at the Roswell Park Memorial Institute (RPMI) 1640 nutrient medium (Sigma Aldrich). The nutrient medium was supplemented with 10% heat inactivated fetal calf serum (FCS) (Sigma Aldrich), 4-(2-

hydroxyethyl)piperazine-1-ethanesulfonic acid (HEPES) (25 mM), penicillin (100 units/mL), streptomycin (200 µg/mL) and L-glutamine (3 mM). Cells were maintained as a monolayer culture in tissue culture flasks (Thermo Scientific Nunc™), in an incubator at 37 °C, in a humidified atmosphere composed of 5% CO<sub>2</sub>.

**2.4.2. MTT cytotoxicity assay.** The antiproliferative activity of the tested complexes was determined using the 3-(4,5-dimethylthiazol-yl)-2,5-diphenyltetrazolium bromide (MTT, Sigma Aldrich) assay [48]. Cells were seeded into 96-well cell culture plates (Thermo Scientific Nunc™), in number of 4000 c/w (HeLa), 7000 c/w (LS-174 and MRC-5) and 8000 c/w (A549), in 100 µL of culture medium. After 24 h of growth, cells were exposed to serial dilutions of tested agents. Stock solutions were prepared immediately prior to use by dissolving in DMSO, so that the DMSO content did not exceed 1% (v/v). The antiproliferative effects of the complexes and ligands were evaluated in concentrations up to 200 µM for 72 h of continuous drug action. After treatment, 20 µL of MTT solution, 5 mg/mL in phosphate buffer solution (PBS), pH 7.2, was added to each well. The samples were incubated for 4 h at 37 °C with 5% CO<sub>2</sub> in humidified atmosphere. Formazan crystals were dissolved in 100 µL of 10% sodium dodecyl sulfate (SDS). The absorbance was recorded on a microplate reader (ThermoLabsystems Multiskan EX 200e240 V) after 24 h at a wavelength of 570 nm. The IC<sub>50</sub> value (µM) was defined as the concentration of a drug which produces 50% inhibition of cell survival and was determined based on the cell survival diagrams.

**2.4.3. Combinational drug study.** N-acetyl-L-cysteine (NAC) and L-buthionine-sulfoximine (L-BSO) were purchased from Sigma-Aldrich. NAC and L-BSO were dissolved in a physiological saline solution, at a final concentration of 30 mM, and sterilized by filtration (0.2 µm pore-size filters). The stock solutions were wrapped in foil and kept at -20 °C.

*2.4.3.1. Effects of N-acetyl-L-cysteine (NAC) or L-buthionine-sulfoximine (L-BSO) on 2 - treated HeLa cells in relation to cell survival.* In the combinational study, L-buthionine-sulfoximine (L-BSO) or N-acetyl-L-cysteine (NAC) was used in pre-treatment with **2**. Briefly, HeLa cells were pre-treated with subtoxic concentrations of L-BSO (1 µM) or NAC (20 µM) for 3 h, and after washing out, the treatment continued with **2** alone, applied in selected concentrations (50,



100, 200  $\mu\text{M}$ ). Viability of HeLa cells, after 72 h of continual treatment with **2** alone, or in combination with NAC (20  $\mu\text{M}$ )/L-BSO (1  $\mu\text{M}$ ), was measured by MTT (3-(4,5-dimethylthiazol-2-yl)-2,5-diphenyltetrazolium bromide) assay, as previously described.

*2.4.3.2. Effects of N-acetyl-L-cysteine (NAC) or L-buthionine-sulfoximine (L-BSO) on 2 - treated HeLa cells in relation to cell cycle perturbations.* Cell cycle phase distribution analysis was performed by flow-cytometry of the DNA content in fixed HeLa cells after staining with propidium iodide (PI) [49]. The cells were seeded at a density of  $2 \times 10^5$  cells/well in 6-well plates and growth in nutrition medium. After 24 h, the cells were exposed to NAC (20  $\mu\text{M}$ ) or L-BSO (1  $\mu\text{M}$ ) for 3 h, and after washing out, the cells were continually exposed to **2** for 48 h with  $\text{IC}_{50}$  (132  $\mu\text{M}$ ) concentration. Control cells were incubated only in nutrient medium. After 48 h of continual treatment, the cells were collected by trypsinization, washed twice with ice-cold PBS, and fixed for 30 min in 70% EtOH. After fixation, the cells were washed again with PBS and incubated with RNaseA (1 mg/mL) for 30 min at 37 °C. The cells were then stained with PI (400  $\mu\text{g}/\text{mL}$ ) 15 min before flow-cytometric analysis. Cell cycle phase distributions were analyzed using a fluorescence activated cell sorting (FACS) Calibur Becton Dickinson flow cytometer and Cell Quest computer software.

## **2.5. DNA-binding studies**

DNA (isolated from salmon testes) was purchased from Sigma Aldrich. The studies were performed for **2**.

**2.5.1. UV-vis study.** The absorption titration measurements were performed using a Varian spectrophotometer from 300-800 nm. The complex concentration was fixed at 20 ppm in PBS at pH 7, and titration was done with different aliquots of DNA standard solution to make DNA concentrations of 0, 20, 50, 100, 150 and 250 ppm. After preparing complex-DNA solutions they were allowed to incubate for 5 min at room temperature before the adsorption spectra were recorded.

**2.5.2. Cyclic voltammetry interaction study.** Cyclic voltammetry measurements were done in the same concentration range 0-250 ppm of the DNA presented in the phosphate buffer solution

of 20 ppm of **2**. The voltammetric measurements were performed using a potentiostat/galvanostat (AUTOLAB PGSTAT 302 N, Metrohm Autolab B.V., The Netherlands) controlled by the corresponding electrochemical software (NOVA 1.9). The cell (10 mL) consisted of a three-electrode system, a boron-doped diamond electrode (Windsor Scientific Ltd., Slough, Berkshire, United Kingdom) embedded in a polyether ether ketone (PEEK) body with an inner diameter of 3 mm, a resistivity of 0.075  $\Omega$  cm and a boron doping level of 1000 ppm (as declared by the supplier) as a working electrode, a Ag/AgCl (saturated KCl) as a reference electrode and a Pt wire as a counter electrode. All potentials reported in this paper are referred *versus* the Ag/AgCl (saturated KCl) reference electrode. Also, all experiments were done at ambient temperature after 5 min of incubation period.

### 3. Results and discussion

#### 3.1. Preparation and characterization of 1-4

The general procedure of all the reported complexes included dissolving of the metal precursor and equimolar amount of the ligand in ethanol (scheme 1). The reaction mixture was refluxed for 3 h and then was left to cool to room temperature. After adding the appropriate amount of counterion  $\text{NH}_4\text{PF}_6$  to the solution, intensive color change from dark purple to dark red was observed. Isolated amorphous precipitate was rinsed with a small amount of water and diethylether. Obtained compounds were air stable and showed no traces of decomposition. Complexes **1-4** were soluble in some polar (*e.g.*, DMSO,  $\text{CHCl}_3$ ,  $\text{CH}_2\text{Cl}_2$ ,  $\text{CH}_3\text{CN}$ ) and insoluble in apolar solvents with **1** and **2** very soluble in water.

IR spectra of **1-4** generally revealed an asymmetric stretching vibration that originates from the C=O bond and is located between 1645 and 1650  $\text{cm}^{-1}$ . The coordination of the metal center *via* oxygen is suggested by comparison to the band of the free carboxylic group at  $\sim 1700 \text{ cm}^{-1}$  in spectra of the corresponding ligand(s). The very intense vibration found at 840  $\text{cm}^{-1}$  is assigned to C–H stretches. In ESI-MS spectra of **1-4** recorded in acetonitrile, the  $[\text{M}^+ - \text{PF}_6^-]$  signal was detected.

As for  $^1\text{H}$  NMR, all products share a common structural feature, *i.e.* aromatic protons originating from pyridine and bipyridine moieties. In the  $^1\text{H}$  NMR spectra of **1** and **2**, the  $\text{CH}_3$ -groups in positions 3 and 6 show well-defined singlets at 2.67 and 1.68 ppm, respectively.

All characterization spectra for **1** are presented in Supplementary Material (figures S1-S3).

### 3.2. Single crystal structure analysis

Complex **3** crystallized in the monoclinic centrosymmetric space group  $P2_1/n$  and the asymmetric unit contains one  $[\text{Ru}(5\text{-bromopyridine-2-carboxylate})(\text{bpy})_2]^+$  complex cation, one  $\text{PF}_6^-$  and two ethanol molecules. The  $\text{Ru}^{2+}$  is coordinated to five nitrogens and one oxygen in a distorted octahedron. The Ru-N(bpy) distances are 2.042(2)-2.058(3) Å, while the Ru-N(L) and Ru-O distances are 2.070(2) Å and 2.095(2) Å, respectively (figure 1, table 1). The pairs of pyridine rings in the two bpy ligands are almost planar and show dihedral angles of 4.01(16)° and 1.70(15)°, respectively (between least-squares planes through the respective rings). The pyridine bromine forms C-Br $\cdots\pi$  interactions with the symmetry-equivalent pyridine ring N3/C11-C15 (C-Br $\cdots$ centroid distance of 3.6545(14) Å).

In the packing, several  $\pi$ - $\pi$  stacking interactions are observed between the five pyridine rings (centroid $\cdots$ centroid distances of 3.7820(18)-5.9751(18) Å). Additionally, C-H $\cdots\pi$  interactions are observed between C29(H) and pyridine ring N1/C1-C5(C(H) $\cdots$ centroid distances of 3.508(4) Å). The crystal packing is stabilized by several hydrogen bonds, *i.e.* between the 5-bromopyridine-2-carboxylate O2 and an ethanol (O3(H) $\cdots$ O2 = 2.723(4) Å), between the two ethanol solvent molecules (O4(H) $\cdots$ O3 = 2.874(4) Å) and a longer hydrogen bond between the 5-bromopyridine-2-carboxylate Br1 atom and the latter ethanol molecule (O4(H) $\cdots$ Br1 = 3.466(3) Å) (figure 2).

Compound **4** crystallized in the monoclinic centrosymmetric space group  $I2/a$  and the asymmetric unit contains one  $[\text{Ru}(6\text{-bromopyridine-2-carboxylate})(\text{bpy})_2]^+$  complex cation and one  $\text{PF}_6^-$ . Analogous to **3**, the Ru center is coordinated in a distorted octahedral manner to five nitrogens and one oxygen, with Ru-N(bpy) distances of 2.046(4)-2.056(4) Å, comparable with symmetrical  $[\text{Ru}(\text{bpy})_3]$  complexes in the Cambridge Structural Database (CSD, Version 5.37, 2016) [50], while the Ru-N(L) distance is longer (2.123(4) Å) and the Ru-O distance is 2.077(4) Å (figure 3, table 1).

The pairs of pyridine rings in the two bpy ligands are also almost planar and show dihedral angles of 4.6(3)° and 5.7(3)°, respectively (between least-squares planes through the respective rings). The pyridine bromine forms C-Br $\cdots\pi$  interactions with pyridine ring

N2/C6-C10 and the symmetry-equivalent pyridine ring N3/C11-C15 (C-Br...centroid distance of 3.477(2) Å and 3.887(2) Å, respectively).

In the packing, several  $\pi$ - $\pi$  stacking interactions are observed between the five pyridine rings (centroid...centroid distances of 4.276(3)-5.866(3) Å). Additionally, C-H... $\pi$  interactions are observed between C5(H) and C12(H) and pyridine rings (C(H)...centroid distances of 3.729(6) Å and 3.553(6) Å, respectively).

### 3.3. Electrochemistry

The results obtained from electrochemical measurements are presented in table 2 and representative voltammograms are given in figure 4. For all complexes first reversible oxidation peaks were obtained in the potential range of  $E_{1/2} = -0.02$  V to 0.04 V [51]. Also, all complexes showed a reversible oxidation peak at the potential range of  $E_{1/2} = 0.54$  V to 0.64 V where peak potential shifts depend on the strength of the anionic ligand introduced in the Ru center. Additionally, **1** displayed one irreversible anodic peak at a potential of + 0.81 V which could be attributed to the oxidation of the ligand. In the negative range of potentials, all complexes showed a reversible reduction couple of  $E_{1/2} = -1.02$  V to -1.03 V which could be assigned to reduction of a bipyridine moiety [51]. A second reversible reduction for all complexes was observed at  $E_{1/2} = -1.65$  V to -1.70 V, which could be considered also as reduction of a bipyridine group. A third redox couple was observed at  $E_{1/2} = -1.95$  V to -2.01 V, which in the case of Br-subunits (**4** and **3**) showed quasi-reversible behavior, and could be attributed to the third reduction of bipyridine [22]. For **4**, the irreversible reduction peak at -2.23 V was not observed, which is obtained for all other complexes at the same potential, originating from the reduction of the R-ligands.

### 3.4. Biological activity

**3.4.1. Results of MTT assay.** Cytotoxicities of the ruthenium complexes were determined by MTT assay in three tumor cell lines HeLa, LS-174, A549, and one normal cell line MRC-5. Results obtained after 72 h of drug action are presented in terms of  $IC_{50}$  values (table 3). The complexes exhibited moderate cytotoxic activity in HeLa cells, with  $IC_{50}$  values ranging from  $132 \pm 5$   $\mu$ M (**2**) to  $184 \pm 16$   $\mu$ M (**3**). Complex **2** with the highest cytotoxic activity in HeLa was also the only one to exhibit cytotoxic activity in LS-174 cells ( $180 \pm 10$   $\mu$ M). For coordinatively

saturated, substitutionally inert ruthenium(II) polypyridine complexes, noncovalent association with cellular targets such as DNA is generally assumed to be the primary mode of interaction with biological systems [52, 53]. As compared to the first generations of platinum-based drugs (*cisplatin*, *oxaliplatin*), ruthenium polypyridine complexes possess structural properties that allow differential modes of binding to DNA, like specific covalent cross-linking [54], or intercalation between adjacent nucleobases. However, physicochemical parameters, such as complex stability, and ligand dissociation kinetics, also play important roles in determining their capability to reach target sites in the cell [55]. Few studies provided evidence that ruthenium polypyridine complexes are transported to the interior of the cells, but may remain associated with the cell membrane, particularly if they carry extended and rigid polypyridine ligands [56, 57]. Sterically demanding ligands, such as polycyclic aromatic molecules (polypyridines), were shown to enhance cytotoxicity of ruthenium complexes, due to the hydrophobic interactions with DNA nucleobases or other targets in the cell. Moderate cytotoxicity of **1-4** in the present study may be due to the greater off-target reactivity in solution. Still, minor variations in the structure of the co-ligand(s) resulted in variations in the IC<sub>50</sub> values in HeLa cells. Further investigations of the mechanism of action and of the structure-activity relationship of this class of ruthenium complexes are important for optimization of their activity.

**3.4.2. Effects of NAC or L-BSO on cell survival of HeLa cells treated with 2.** Taking into account the redox activity of Ru compounds bearing bipyridine moieties [22, 40], we investigated whether cytotoxic potential of **2** in HeLa cells could be altered in combination with pharmacological modulators of cell redox-homeostasis, such as L-buthionine-sulfoximine (L-BSO) or N-acetyl-L-cysteine (NAC) [1, 2, 29, 58]. Glutathione, present in millimolar intracellular concentrations, is a major determinant of cellular redox status. L-BSO is a specific inhibitor of  $\gamma$ -glutamylcysteine synthesis ( $\gamma$ -GCS), the rate-limiting enzyme for biosynthesis of glutathione (GSH). N-acetyl-L-cysteine (NAC) is a GSH precursor and is effective in protecting cells from reactive oxygen species (ROS) mediated cytotoxicity [59].

A preliminary dose-response study of L-BSO or NAC, for 72 h action in HeLa cells, was performed. Results showed 22% decrease of cell survival in the concentration range above 2.5  $\mu$ M of L-BSO or above 30  $\mu$ M of NAC (results not presented). Therefore, sub-toxic concentrations of L-BSO (1  $\mu$ M) or NAC (20  $\mu$ M) were selected for further combinational drug

study [60, 61]. However, pretreatment of HeLa cells (3 h) with BSO or NAC did not significantly alter cell response to the action of **2** (figure 5). Results suggested that ROS and GSH might not be closely related to the mechanism of antiproliferative action of **2** in HeLa cells.

**3.4.3. Effects of NAC or L-BSO on 2-induced cell cycle perturbations in HeLa cells.** We performed further combinational drug study to investigate whether pretreatment of HeLa cells by NAC (20  $\mu$ M) or L-BSO (1  $\mu$ M) may affect cell cycle perturbations, caused by **2**. Sub-toxic concentrations of NAC or L-BSO did not affect the cell cycle profile in HeLa cells, compared to the non-treated cells (figure 6). Complex **2** at IC<sub>50</sub> concentration (132  $\mu$ M) induced slight cell cycle perturbations characterized by the increase of sub-G1 content (7.57% compared to control 1.23%), decrease of cell number in G1 phase (52.17%, compared to control 64.66%), and arrest in the S phase (21.40% relative to control 10.99%). Slower progression of cells through S phase of the cell cycle clearly indicated potential of **2** to inhibit replication in HeLa cells, through DNA-interactions or by indirect manner (ROS production). Pre-treatment of HeLa cells with NAC (3 h) caused almost no alterations of cell cycle progression, compared to the action of **2**, as a single agent (figure 6). On the other hand, pretreatment with L-BSO caused more pronounced changes in Sub-G1 phase (increase to 24.21%), as well as in G1 phase (decrease of cell number to 42.23%) (figure 6). It seems that L-BSO at sub-toxic concentrations potentiated apoptotic stimuli caused by **2**. This result suggested that intracellular glutathione may affect action of **2** or may at least influence its intracellular availability for interaction with potential cellular targets.

## **4. Interaction of 2 with DNA**

### **4.1. UV-vis spectroscopy**

Potential interaction of **2** with DNA was studied in PBS at room temperature and the corresponding absorption spectrum in the absence and presence of DNA is shown in figure 7. A band at 355 nm can be assigned to intraligand  $\pi$ - $\pi^*$  transitions while a broad band in the visible region at 462 nm is attributed to the metal-to-ligand charge transfer (MLCT) transitions [62]. As the concentration of DNA increased, both absorption bands displayed clear hypochromism but no obvious red-shift. This observation is in agreement with recently published reports [63, 64]. These studies suggested intercalation for complex-DNA interaction, which usually results in

hypochromism and bathochromism as a direct consequence of interaction between the aromatic chromophore and the base pairs of DNA.

#### 4.2. Cyclic voltammetry

Electrochemical measurements were performed for **2** as a complement for UV-vis spectroscopic investigation of complex-DNA interaction. Cyclic voltammograms were recorded in the presence of increasing amounts of **2** (figure 8). After addition of DNA, two reversible one-electron redox processes are detected. Shifts of  $E_{1/2}$  toward more positive values in a positive potential range ( $0.2 < E_{1/2} < 0.9$  V) indicate ability of this Ru(II) complex to interact with DNA as a result of intercalation [65].

#### 5. Conclusion

New ruthenium(II) bipyridine complexes,  $[\text{Ru}(\text{bpy})_2\text{L}](\text{PF}_6)$  (L = 3-methylpyridine-2-carboxylic acid, 6-methylpyridine-2-carboxylic acid, 5-bromopyridine-2-carboxylic acid and 6-bromopyridine-2-carboxylic acid), were synthesized and characterized by various methods including X-ray crystallography for **3** and **4**. Electrochemical properties of the synthesized complexes were investigated. Complexes **1-4** showed moderate cytotoxicities, which may be due to unfavorable ligand dissociation kinetics and off-target reactivity in solution.

Still, minor variations in the structure of the co-ligand resulted in variations in the resulting  $\text{IC}_{50}$  values obtained in HeLa cells. Complex **2** exhibited the highest activity in cervical cancer HeLa cells, with  $\text{IC}_{50}$  value being  $132 \pm 5$   $\mu\text{M}$ . Combinational drug studies revealed that L-BSO did not affect cytotoxicity of **2**, though it modulated its effect on the cell cycle by enhancing arrest in the S phase and increasing Sub-G1 peak (fragmented DNA). Among ruthenium compounds bearing polypyridine moieties, several have proven to be mitochondria-targeting anticancer drug candidates, which often induce redox reactions inside cancer cells, resulting in an increase of reactive oxygen species (ROS) [58, 61, 66, 67]. However, combinational drug studies using the ROS scavenger NAC did not affect the activity of **2**. For investigation of the binding mode of **2** to DNA, UV-vis and cyclic voltammetry were employed. Both techniques suggest an intercalative binding. Our results are in agreement to previous reports on ruthenium(II) bipyridine complexes, indicating that DNA binding behavior is an important aspect of their biological action [68, 69]. However, it is also evident that ruthenium(II)

complexes bearing different ligands show different cellular distribution [70, 71]. In conclusion, even subtle changes in the molecular structures of ruthenium polypyridine complexes may give substantial contribution to their binding modes, sites, and affinities, *in vitro*.

### Appendix A. Supplementary data

CCDC 1482372-1482373 contain the supplementary crystallographic data for this paper and can be obtained free of charge via [www.ccdc.cam.ac.uk/conts/retrieving.html](http://www.ccdc.cam.ac.uk/conts/retrieving.html) (or from the Cambridge Crystallographic Data Centre, 12 Union Road, Cambridge CB2 1EZ, UK; Fax: +44-1223-336033; or [deposit@ccdc.cam.ac.uk](mailto:deposit@ccdc.cam.ac.uk)). Supplementary data associated with this article can be found in the online version.

### Funding

This research was supported by Ministry of Education, Science and Technological Development of the Republic of Serbia [Project numbers: 172035, III41026]. The authors also acknowledge the support of the FP7 RegPot project FCUB ERA GA [Project number 256716]. The EC does not share responsibility for the content of this article. KVH thanks the Hercules Foundation (project AUGÉ/11/029 "3D-SPACE: 3D Structural Platform Aiming for Chemical Excellence") and the Research Fund-Flanders (FWO) for funding.

### References

- [1] M. Gielen, E.R.T. Tiekink, *Metallotherapeutic Drugs and Metal-based Diagnostic Agents*, John Wiley & Sons Ltd., Chichester (2005).
- [2] M.A. Jakupec, M. Galanski, V.B. Arion, C.G. Hartinger, B.K. Keppler. *Dalton Trans.*, 183 (2008).
- [3] G. Gasser, I. Ott, N. Metzler-Nolte. *J. Med. Chem.*, **54**, 3 (2011).
- [4] B. Rosenberg, L. Van Camp, T. Krigas. *Nature*, **205**, 698 (1965).
- [5] B. Rosenberg, L. Van Camp, J.E. Trosko, V.H. Mansour. *Nature*, **222**, 385 (1969).
- [6] Z.H. Siddik. *Oncogene*, **22**, 7265 (2003).
- [7] E. Wong, C.M. Giandomenico. *Chem. Rev.*, **99**, 2451 (1999).
- [8] A. Bergamo, G. Sava. *Dalton Trans.*, **40**, 7817 (2011).



- [9] L. Messori, L. Marchetti, L. Massai, F. Scaletti, A. Guerri, I. Landini, S. Nobili, G. Perrone, E. Mini, P. Leoni, M. Pasquali, C. Gabbian. *Inorg. Chem.*, **53**, 2396 (2014).
- [10] A.R. Kapdi, I.J.S. Fairlamb. *Chem. Soc. Rev.*, **43**, 4751 (2014).
- [11] M. Hanif, M.V. Babak, C.G. Hartinger. *Drug Discov. Today*, **19**, 1640 (2014).
- [12] A.J. Di Pasqua, J. Goodisman, J.C. Dabrowiak. *Inorg. Chim. Acta*, **389**, 29 (2012).
- [13] F. Montagnani, G. Turrisi, C. Marinozzi, C. Aliberti, G. Fiorentini. *Gastric Cancer*, **14**, 50 (2011).
- [14] A. Kurzwernhart, W. Kandioller, É.A. Enyedy, M. Novak, M.A. Jakupec, B.K. Keppler, C.G. Hartinger. *Dalton Trans.*, **42**, 6193 (2013).
- [15] K. Suntharalingam, W. Lin, T.C. Johnstone, P.M. Bruno, Y.R. Zheng, M.T. Hemann, S.J. Lippard. *J. Am. Chem. Soc.*, **136**, 14413 (2014).
- [16] A. Habtemariam, M. Melchart, R. Fernández, S. Parsons, I.D.H. Oswald, A. Parkin, F.P.A. Fabbiani, J.E. Davidson, A. Dawson, R.E. Aird, D.I. Jodrell, P.J. Sadler. *J. Med. Chem.*, **49**, 6858 (2006).
- [17] A. Bergamo, G. Sava. *Chem. Soc. Rev.*, **44**, 8818 (2015).
- [18] F. Bacher, V.B. Arion, Elsevier Reference Module in Chemistry, Molecular Sciences and Chemical Engineering, Elsevier, Waltham, MA (2014), <http://dx.doi.org/10.1016/B978-0-12-409547-2.11353-8>.
- [19] T. Gianferrara, I. Bratsos, E. Alessio. *Dalton Trans.*, 7588 (2009).
- [20] B. Bertrand, A. Casini. *Dalton Trans.*, **43**, 4209 (2014).
- [21] J.J. Wilson, S.J. Lippard. *Inorg. Chem.*, **50**, 3103 (2011).
- [22] S. Bellinger-Buckley, T. Chang, S. Bag, D. Schweinfurth, W. Zhou, B. Torok, B. Sarkar, M. Tsai, J. Rochford. *Inorg. Chem.*, **53**, 5556 (2014).
- [23] J.M. Lazić, L.J. Vučićević, S. Grgurić-Šipka, K. Janjetović, G.N. Kaluđerović, M. Misirlić, M. Gruden-Pavlović, D. Popadić, R. Paschke, V. Trajković, T. Sabo. *ChemMedChem*, **5**, 881 (2010).
- [24] A. Savić, L. Filipović, S. Arandelović, B. Dojčinović, S. Radulović, T.J. Sabo, S. Grgurić-Šipka. *Eur. J. Med. Chem.*, **82**, 372 (2014).
- [25] P. Nagababu, A.K. Barui, B. Thulasiram, C.S. Devi, S. Satyanarayana, C.R. Patra, B. Sreedhar. *J. Med. Chem.*, **58**, 5226 (2013).

- [26] A. Savić, M. Dulović, J. M. Poljarević, S. Misirlić-Denčić, M. Jovanović, A. Bogdanović, V. Trajković, T.J. Sabo, S. Grgurić-Šipka, I. Marković. *ChemMedChem*, **6**, 1884 (2011).
- [27] J. Kljun, I. Bratsos, E. Alessio, G. Psomas, U. Repnik, M. Butinar, B. Turk, I. Turel. *Inorg. Chem.*, **52**, 9039 (2013).
- [28] I. Turel. *Coord. Chem. Rev.*, **232**, 27 (2002).
- [29] J.A. Fernandez-Pol, D.J. Klos, P.D. Hamilton. *Anticancer Res.*, **21**, 3773 (2001).
- [30] S. Cai, K. Sato, T. Shimizu, S. Yamabe, M. Hiraki, C. Sano, H. Tomioka. *J. Antimicrob. Chemoth.*, **57**, 85 (2006).
- [31] R.S. Grant, S.E. Coggan, G.A. Smythe. *Int. J. Tryptophan Res.*, **2**, 71 (2009).
- [32] T. Rebello, B. Lonnerdal, L.S. Hurley. *Am. J. Clin. Nutr.*, **35**, 1 (1982).
- [33] T.O. Berner, M.M. Murphy, R. Slesinski. *Food Chem. Toxicol.*, **42**, 1029 (2004).
- [34] M. Peng, X. Yang. *J. Inorg. Biochem.*, **146**, 97 (2015).
- [35] A. Pérez, L. Hernández, E. Del Carpio, V. Lubes. *J. Mol. Liq.*, **194**, 193 (2014).
- [36] D.M. Steams, W.H. Armstrong. *Inorg. Chem.*, **31**, 5178 (1992).
- [37] R. Song, K.M. Kim, Y.S. Sohn. *Inorg. Chim. Acta*, **292**, 238 (1999).
- [38] I. Ivanović, K.K. Jovanović, N. Gligorijević, S. Radulović, V.B. Arion, K.S.A.M. Sheweshein, Ž.Lj. Tešić, S. Grgurić-Šipka. *J. Organomet. Chem.*, **749**, 343 (2014).
- [39] N. Gligorijević, S. Arandelović, L. Filipović, K. Jakovljević, R. Janković, S. Grgurić-Šipka, I. Ivanović, S. Radulović, Ž.Lj. Tešić. *J. Inorg. Biochem.*, **108**, 53 (2012).
- [40] Y. Zhang, L. Lai, P. Cai, G. Cheng, X. Xu, Y. Liu. *New J. Chem.*, **39**, 5805 (2015).
- [41] J.Q. Wang, P.Y. Zhang, L.N. Ji, H. Chao. *J. Inorg. Biochem.*, **146**, 89 (2015).
- [42] H. Ohtsu, K. Tanaka. *Angew. Chem. Int. Ed.*, **51**, 9792 (2012).
- [43] B.P. Sullivan, D.J. Salmon, T.J. Meyer. *Inorg. Chem.*, **17**, 3334 (1978).
- [44] A. Savić, A.A. Baroud, S. Grgurić-Šipka. *Maced. J. Chem. Chem. En.*, **33**, 59 (2014).
- [45] Rigaku Oxford Diffraction. *CrysAlis PRO*. Rigaku Oxford Diffraction, Yarnton, England (2015).
- [46] O.V. Dolomanov, L.J. Bourhis, R.J. Gildea, J.A.K. Howard, H. Puschmann, *OLEX2: A complete structure solution, refinement and analysis program. J. Appl. Crystallogr.*, **42**, 339 (2009).
- [47] G.M. Sheldrick. A short history of *SHELX*, *Acta Cryst.*, **A64**, 112 (2008).

- [48] R. Supino, *In Vitro Toxicity Testing Protocols*, S. O'Hare, C.K. Atterwill (Eds.), pp. 137, Humana Press, New Jersey (1995).
- [49] M.G. Ormerod, *Flow Cytometry, a Practical Approach*, M.G. Ormerod (Ed.), 3<sup>rd</sup> Edn., pp. 119, Oxford University Press, New York (1994).
- [50] F.H. Allen. *Acta Cryst.*, **B58**, 380 (2002).
- [51] D. Cabral, P.C. Howlett, J.M. Pringle, X. Zhang, D. MacFarlane. *Electrochim. Acta*, **180**, 419 (2015).
- [52] A.C.G. Hotze, S.E. Caspers, D. de Vos, H. Kooijman, A. Spek, Flamigni, M. Bacac, G. Sava, J.G. Haasnoot, J. Reedijk. *J. Biol. Inorg. Chem.*, **9**, 354 (2004).
- [53] L. Mishra, A.K. Yadaw, R. Sinha, A.K. Singh. *Indian J. Chem. Sect. A-Inorg. Bio-Inorg. Phys. Theor. Anal. Chem.*, **40**, 913 (2001).
- [54] L. Marcélis, C. Moucheron, A. Kirsch-De Mesmaeker. *Philos. Trans. A. Math. Phys. Eng. Sci.*, **371**, 20120131 (2013).
- [55] P.C.A. Bruijninch, P.J. Sadler, *Advances in Inorganic Chemistry*, R. van Eldik, C.D. Hubbard (Eds.), Vol. 61, pp. 1 (2009).
- [56] C.A. Puckett, J.K. Barton. *J. Am. Chem. Soc.*, **129**, 46 (2007).
- [57] C.A. Puckett, J.K. Barton. *Biochemistry*, **47**, 11711 (2008).
- [58] S.G. Menon, M.C. Coleman, S.A. Walsh, D.R. Spitz, P.C. Goswami. *Antioxid. Redox Signal.*, **7**, 711 (2005).
- [59] H.H.W. Chen, M.T. Kuo. *Met.-Based Drugs*, **2010**, 1 (2010).
- [60] Y.H. Han, S.Z. Kim, S.H. Kim, W.H. Park. *Int. J. Oncol.*, **33**, 205 (2008).
- [61] Y. Fu, A. Habtemariam, A.M.B.H. Basri, D. Braddick, G.J. Clarkson, P.J. Sadler. *Dalton Trans.*, **40**, 10553 (2011).
- [62] X.W. Liu, Y.M. Shen, Z.X. Li, X. Zhong, Y.D. Chen, S.B. Zhang. *Spectrochim. Acta, Part A*, **149**, 150 (2015).
- [63] A.M. Pyle, J.P. Rehmann, R. Meshoyrer, C.V. Kumar, N.J. Turro, J.K. Barton. *J. Am. Chem. Soc.*, **111**, 3051 (1989).
- [64] V.R. Putta, R.R. Mallepally, S. Avudoddi, P.K. Yata, N. Chintakuntla, D. Nancherla, K. Nagasuryaprasad, S.S. Surya, S. Sirasani. *Anal. Biochem.*, **485**, 49 (2015).
- [65] X. Totta, A.A. Papadopoulou, A.G. Hatzidimitriou, A. Papadopoulos, G. Psomas. *J. Inorg. Biochem.*, **145**, 79 (2015).

- [66] D. Trachootham, J. Alexandre, P. Huang. *Nat. Rev. Drug Discov.*, **8**, 579 (2009).
- [67] Y. Zhao, Y. Li, P. Luo, Y. Gao, J. Yang, K.-H. Lao, G. Wang, G. Cockerill, Y. Hu, Q. Xu, T. Li, L. Zeng. *Sci. Rep.*, **6**, 1 (2016).
- [68] J. Sun, W.X. Chen, X.D. Song, X.H. Zhao, A.Q. Ma, J.X. Chen. *J. Coord. Chem.*, **68**, 308 (2015).
- [69] C. Wang, Q. Wu, Y. Zeng, D. Huang, C. Yu, X. Wang, W. Mei. *J. Coord. Chem.*, **68**, 1489 (2015).
- [70] Z. Zhang, W. Mei, X. Wu, X. Wang, B. Wang, S. Chen. *J. Coord. Chem.*, **68**, 1465 (2015).
- [71] V. Pierroz, T. Joshi, A. Leonidova, C. Mari, J. Schur, I. Ott, L. Spiccia, S. Ferrari, G. Gasser. *J. Am. Chem. Soc.*, **134**, 20376 (2012).

## Figure captions

Figure 1. Molecular structure of the cation of **3** showing thermal displacement ellipsoids at the 50% probability level and atom labeling scheme of the hetero-atoms. The  $\text{PF}_6^-$  counter anion and two solvent EtOH molecules are omitted for clarity.

Figure 2. Packing in the crystal structure of **3** along the  $a$ -axis. Hydrogen bonds, formed between the 5-bromopyridine-2-carboxylate bromine and carboxyl and the ethanol molecules, are indicated.

Figure 3. Molecular structure of the cation of **4** showing thermal displacement ellipsoids at the 50% probability level and atom labeling scheme of the hetero-atoms. The  $\text{PF}_6^-$  counter anion is omitted for clarity.

Figure 4. The cyclic voltammograms recorded in DMSO (0.1 mM TBAP) at a boron-doped diamond working electrode a) for **1-4** with scan rate  $20 \text{ mV s}^{-1}$  and b) for **1** with scan rate 50, 100, 150, 200, 300, 500  $\text{mV s}^{-1}$ .

Figure 5. Effects of NAC and L-BSO on the cell survival in **2**-treated HeLa cells. Exponentially growing cells were pre-treated with  $20 \mu\text{M}$  NAC or  $1 \mu\text{M}$  L-BSO and then after washing out, further treated with 50, 100 or  $200 \mu\text{M}$  with **2** for 72 h. Bars represent average of triplicates  $\pm$  SD.

Figure 6. Effects of NAC and L-BSO on the cell cycle of **2**-treated HeLa cells. Exponentially growing cells were pre-treated with  $20 \mu\text{M}$  NAC or  $1 \mu\text{M}$  L-BSO and then after washing out, further treated with **2** ( $\text{IC}_{50}$   $132 \mu\text{M}$ ) for 72 h. Bars represent average of duplicates.

Figure 7. Absorption spectra of **2** in DMSO (0.1 mM PBS) at pH 7 upon addition of DNA,  $[\text{Ru}] = 20 \text{ ppm}$ ,  $[\text{DNA}] = 0\text{-}250 \text{ ppm}$ . Arrow shows the absorbance change upon increasing DNA.

Figure 8. The cyclic voltammograms recorded in DMSO (0.1 mM PBS) at a boron-doped electrode upon the addition of **2** ( $[\text{DNA}] = 20 \text{ ppm}$  and  $[\text{2}] = 0\text{-}250 \text{ ppm}$ ) in a potential range a)  $0.0 < E_{1/2} < 1.6 \text{ V}$  and b)  $0.0 < E_{1/2} < 0.9 \text{ V}$ . Arrow shows  $E_{1/2}$  shifts change upon increasing complex concentration.

Table 1. Selected bond lengths (Å) and angles (°) for **3** and **4**.

Selected bond lengths (Å)	<b>3</b>	<b>4</b>
Ru1-N1	2.055(3)	2.046(4)
Ru1-N2	2.042(3)	2.056(4)
Ru1-N3	2.070(3)	2.053(4)
Ru1-N4	2.058(3)	2.048(4)
Ru1-N5	2.069(3)	2.123(4)
Ru1-O1	2.095(2)	2.077(4)
Selected bond angles (°)	<b>3</b>	<b>4</b>
N2-Ru1-N5	94.72(10)	103.36(16)
N2-Ru1-N3	97.81(11)	98.65(17)
N2-Ru1-N4	96.18(10)	92.75(16)
N2-Ru1-N1	79.15(11)	78.96(16)
N5-Ru1-O1	79.83(10)	79.68(14)
N5-Ru1-N3	96.24(10)	90.34(16)
N3-Ru1-O1	89.62(10)	87.35(16)
N4-Ru1-O1	89.74(10)	85.15(15)
N4-Ru1-N3	78.85(10)	79.50(17)
N1-Ru1-O1	93.87(10)	94.80(15)
N1-Ru1-N5	89.31(10)	94.67(16)
N1-Ru1-N4	96.14(10)	95.97(16)

Table 2. Electrochemical data for **1-4** recorded in DMSO (0.1 M TBAP) at a boron-doped diamond electrode with scan rate of 20 mV s<sup>-1</sup>.

$E_{1/2}$ / V (vs. Ag/AgCl)							
	Positive potentials range			Negative potentials range			
	A1 <sub>(ox/red)</sub>	A2 <sub>(ox/red)</sub>	A3 <sub>(ox/red)</sub>	R1 <sub>(ox/red)</sub>	R2 <sub>(ox/red)</sub>	R3 <sub>(ox/red)</sub>	R4 <sub>(ox/red)</sub>
<b>1</b>	0.095/0.014	0.59/0.48	0.81	-1.03/-1.13	-1.64/-1.75	-1.89/-2.01	-2.23
<b>2</b>	0.037/0.038	0.72/0.56	-	-1.00/-1.04	-1.59/-1.68	-1.89/-1.96	-2.23
<b>3</b>	0.04/0.039	0.64/0.058	-	-/-1.09	-1.64/-1.68	-/-1.92	-2.20
<b>4</b>	0.01/-0.04	0.66/0.48	-	-	-1.65/-1.76	-/-2.01	-

ACCEPTED MANUSCRIPT

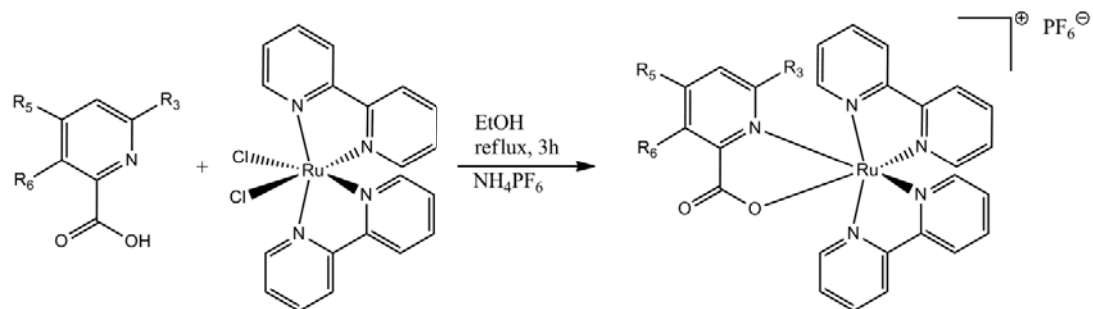
Table 3. Cytotoxicities of the tested agents and *cisplatin* in terms of IC<sub>50</sub> values (μM), obtained for 72 h of continuous drug action, by MTT assay. IC<sub>50</sub> values present average (± SD).

Compound	IC <sub>50</sub> ± SD (μM)*			
	HeLa	A549	LS-174	MRC-5
<b>1</b>	> 200	> 200	> 200	> 200
<b>2</b>	132±5	> 200	180±10	> 200
<b>3</b>	184±16	> 200	> 200	> 200
<b>4</b>	148±8	> 200	> 200	> 200

\*> 200 denotes that IC<sub>50</sub> was not obtained in the range of concentrations tested up to 200 μM.

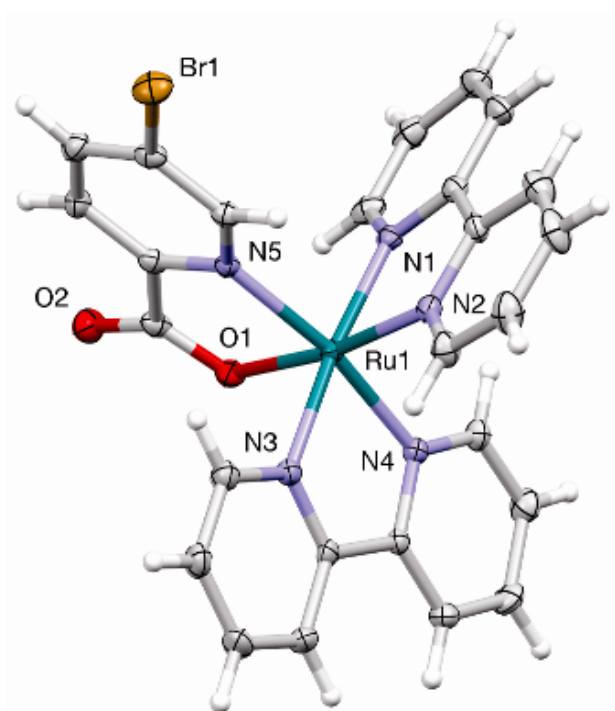
ACCEPTED MANUSCRIPT



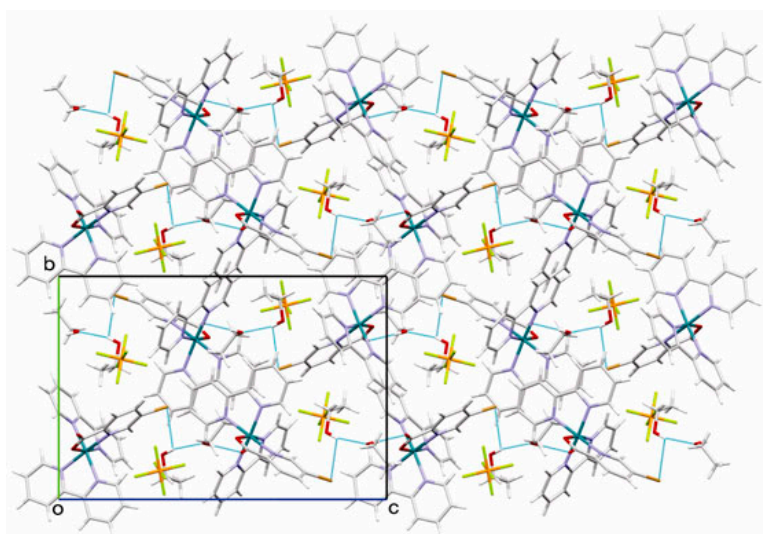


- (1)  $R_3 = \text{CH}_3$ ;  $R_5 = \text{H}$ ;  $R_6 = \text{H}$ ;
- (2)  $R_3 = \text{H}$ ;  $R_5 = \text{H}$ ;  $R_6 = \text{CH}_3$ ;
- (3)  $R_3 = \text{H}$ ;  $R_5 = \text{Br}$ ;  $R_6 = \text{H}$ ;
- (4)  $R_3 = \text{H}$ ;  $R_5 = \text{H}$ ;  $R_6 = \text{Br}$ ;

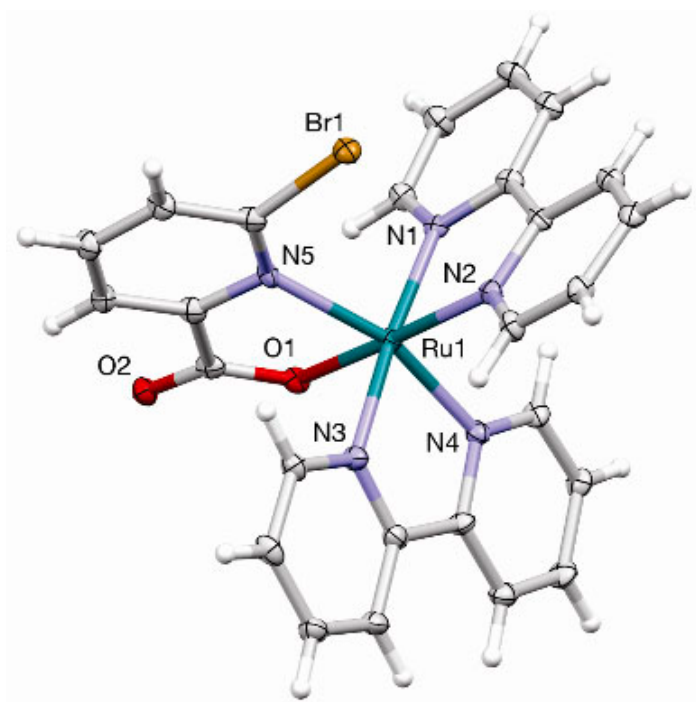
ACCEPTED MANUSCRIPT



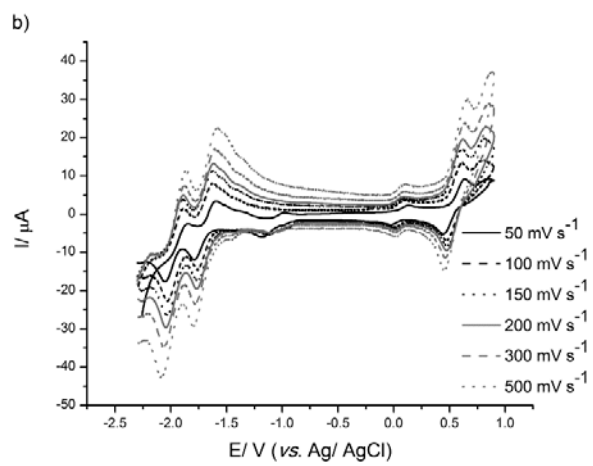
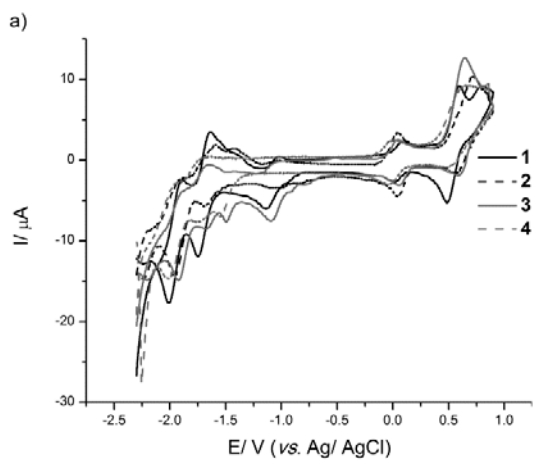
ACCEPTED MANUSCRIPT



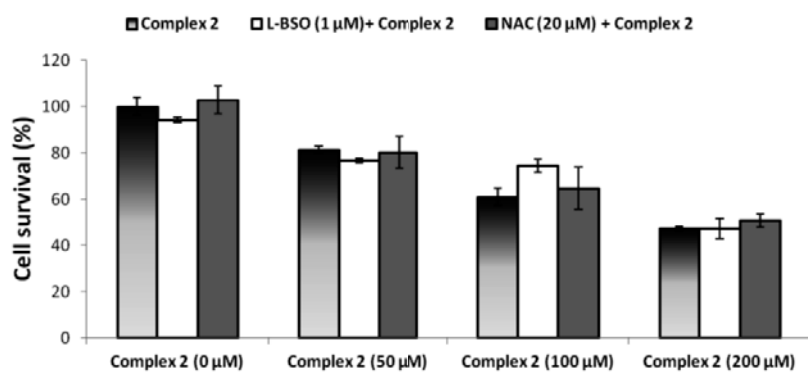
ACCEPTED MANUSCRIPT



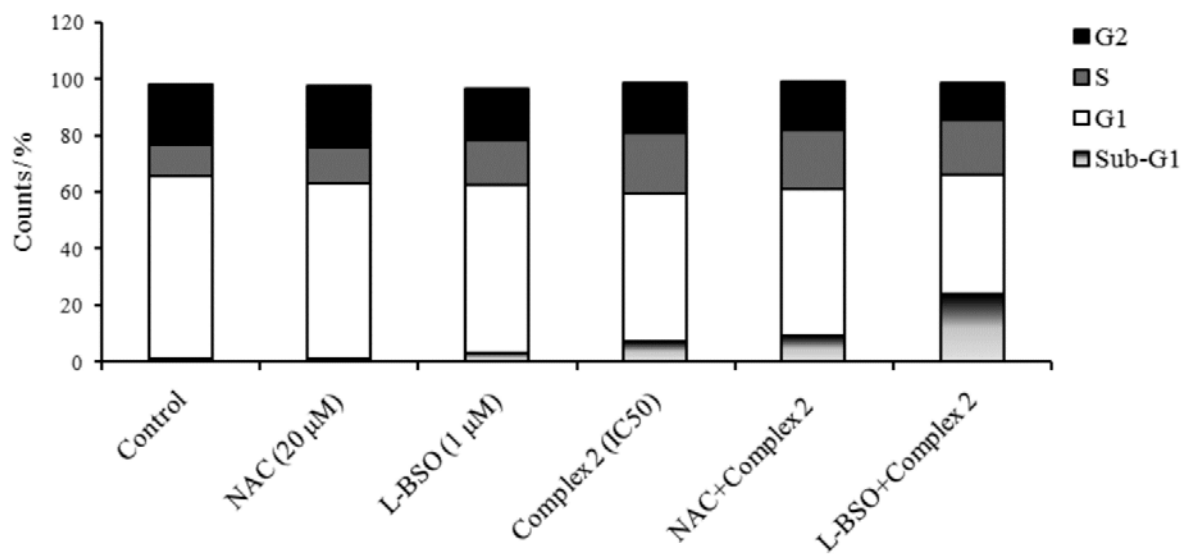
ACCEPTED MANUSCRIPT



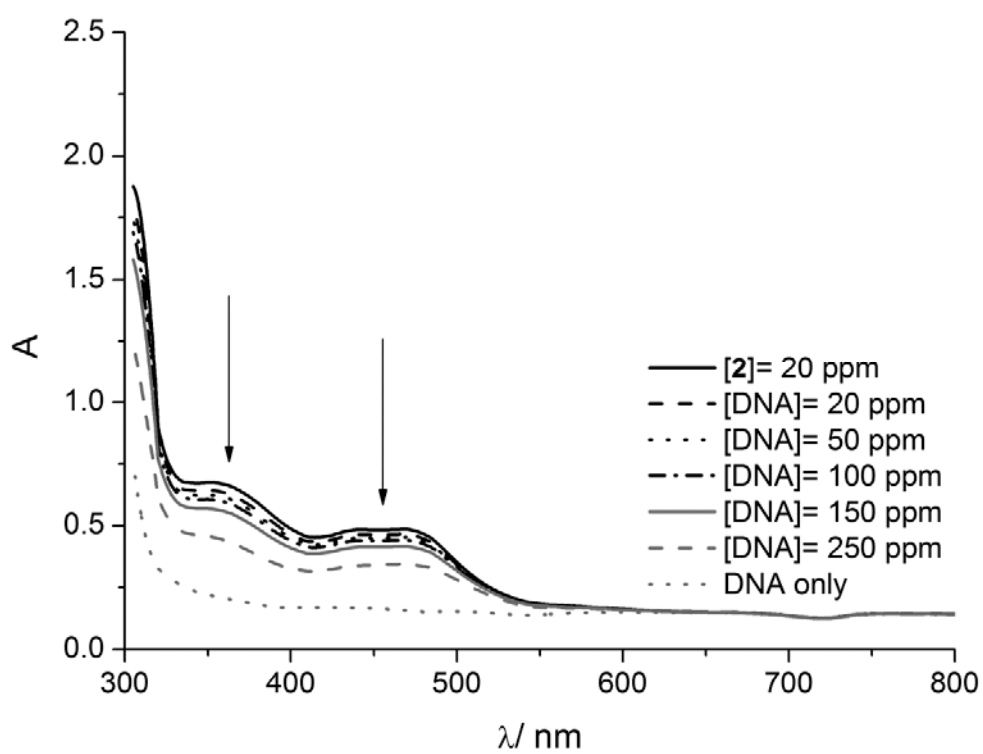
ACCEPTED MANUSCRIPT



ACCEPTED MANUSCRIPT

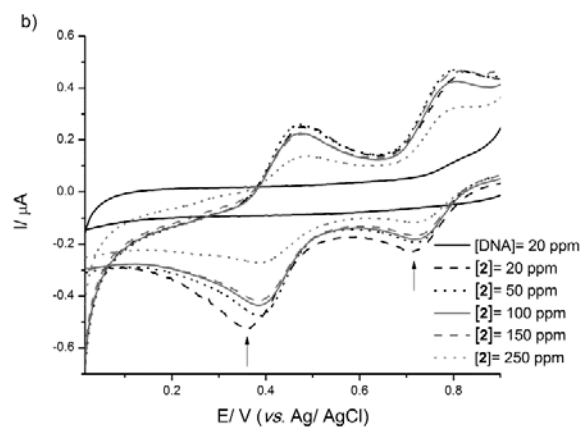
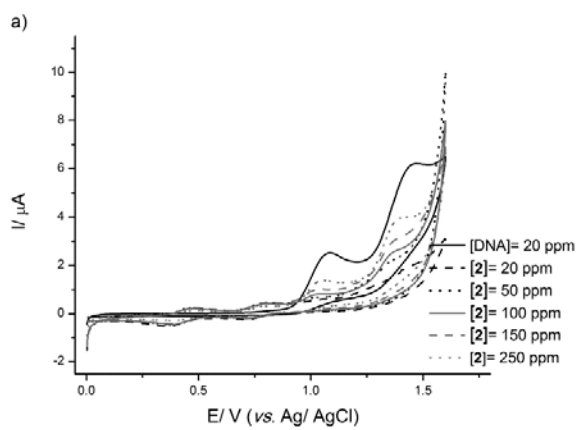


ACCEPTED MANUSCRIPT



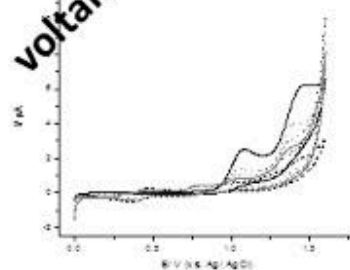
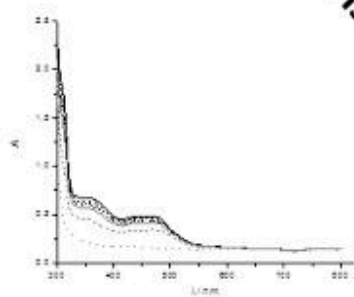
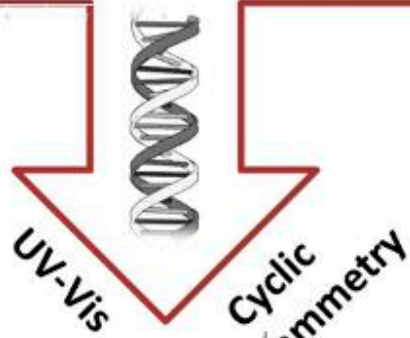
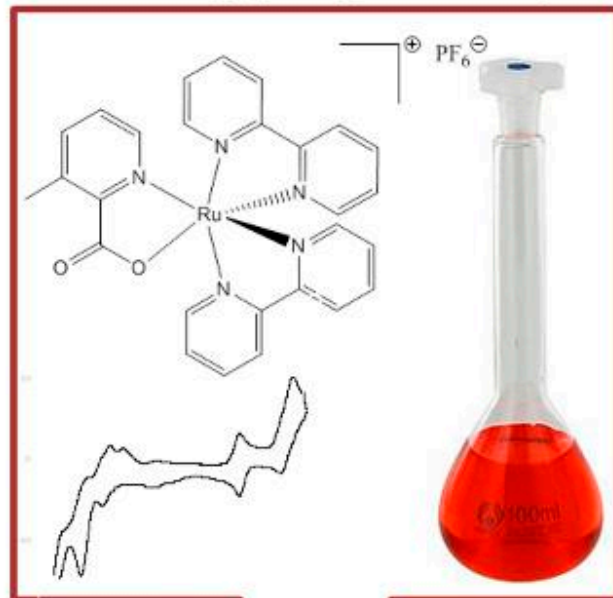
ACCEPTED





ACCEPTED MANUSCRIPT

## Interesting (bio)redox system



AC

RIPT